

## Article

# New Age Constraints of the Bilong Co Oil Shale in the Qiangtang Basin, Northern Tibet: Evidence from In Situ U–Pb Dating and Palaeontology

Haowei Zhang<sup>1,2</sup>, Jian Wang<sup>1,2,3,\*</sup>, Ahmed Mansour<sup>1,2,4</sup> , Jianyong Zhang<sup>5</sup>, Hengye Wei<sup>1,2</sup>, Xiugen Fu<sup>1,2,3</sup>, Lijun Shen<sup>1,2</sup>, Shaoyun Xiong<sup>5</sup>, Mohamed S. Ahmed<sup>6</sup>  and Thomas Gentzis<sup>7,\*</sup> 

<sup>1</sup> School of Geoscience and Technology, Southwest Petroleum University, Chengdu 610500, China; zhanghaowei@163.com (H.Z.); ahmedmans48@mu.edu.eg (A.M.); weihengye@163.com (H.W.); fuxiugen@126.com (X.F.); shenlj9102@163.com (L.S.)

<sup>2</sup> Qiangtang Institute of Sedimentary Basin, Southwest Petroleum University, Chengdu 610500, China

<sup>3</sup> National Key Laboratory of Oil and Gas Reservoir Geology and Exploitation, Southwest Petroleum University, Chengdu 610050, China

<sup>4</sup> Geology Department, Faculty of Science, Minia University, Minia 61519, Egypt

<sup>5</sup> Key Laboratory of Carbonate Reservoirs, CNPC, Hangzhou 310023, China; zhangjy\_hz@petrochina.com.cn (J.Z.); xiong\_yuan\_120@163.com (S.X.)

<sup>6</sup> Geology and Geophysics Department, College of Science, King Saud University, P.O. Box 2455, Riyadh 11451, Saudi Arabia; mohahmed@ksu.edu.sa

<sup>7</sup> Core Laboratories, 6316 Windfern Road, Houston, TX 77040, USA

\* Correspondence: w1962jian@163.com (J.W.); thomas.gentzis@corelab.com (T.G.)

**Abstract:** The Bilong Co oil shale is one of the most significant source rocks in the Mesozoic Qiangtang Basin (Northern Tibet); however, its absolute chronology remains controversial. In this study, in situ carbonate U–Pb isotope dating analysis was carried out for the first time. Detailed field geological investigations yielded some age-diagnostic ammonites, enabling a re-evaluation of the stratigraphic age of the Bilong Co oil shale. A total of 61 spots of U–Pb isotope dating from the middle part of the Bilong Co oil shale section suggests an average age of  $181 \pm 13$  Ma. Elemental geochemistry and diagenetic analysis indicate that the proposed age represents the early deposition of the calcite, and the oil shale was deposited during the Early Jurassic time. This estimated age is further supported by the newly discovered ammonite assemblage of *Hildoceratidae–Tiltoniceras* sp. at the top part of the oil shale section, which confirms the deposition of the oil shale during the Toarcian age of the late Early Jurassic. Consequently, the Bilong Co oil shale can be assigned to the Quse Formation, which is attributed to the Lower Jurassic rather than the Middle Jurassic. The re-assessment of the stratigraphic age of the Bilong Co oil shale is of great significance for regional evaluation and exploration activities of hydrocarbon source rock layers in the Qiangtang Basin as well as for global stratigraphic correlation of the late Early Jurassic Toarcian oceanic anoxic event.

**Keywords:** carbonate U–Pb geochronology; ammonite biostratigraphy; oil shales; Quse Formation; Early Jurassic; Tibetan Plateau



**Citation:** Zhang, H.; Wang, J.; Mansour, A.; Zhang, J.; Wei, H.; Fu, X.; Shen, L.; Xiong, S.; Ahmed, M.S.; Gentzis, T. New Age Constraints of the Bilong Co Oil Shale in the Qiangtang Basin, Northern Tibet: Evidence from In Situ U–Pb Dating and Palaeontology. *Minerals* **2024**, *14*, 246. <https://doi.org/10.3390/min14030246>

Academic Editor: Ricardo Ferreira Louro Silva

Received: 9 January 2024

Revised: 10 February 2024

Accepted: 24 February 2024

Published: 28 February 2024



**Copyright:** © 2024 by the authors. Licensee MDPI, Basel, Switzerland. This article is an open access article distributed under the terms and conditions of the Creative Commons Attribution (CC BY) license (<https://creativecommons.org/licenses/by/4.0/>).

## 1. Introduction

The Early Jurassic (early Toarcian *ca.* 183 Ma) was a time of intense environmental and paleoceanographic perturbations, such as perturbations of the carbon cycle [1,2], global warming [3], accelerated hydrological cycling and intense continental weathering [4–7], high magnitude sea level changes [8], and accumulation of organic-rich sediments such as in the Qiangtang Basin [6,9]. The Qiangtang Basin, located in the eastern Tethyan domain of northern Tibet, is the largest Mesozoic marine hydrocarbon-bearing basin in China [9–12]. The Bilong Co oil shale is one of the main source rocks investigated in the Mesozoic Qiangtang Basin and has received considerable attention in hydrocarbon exploration activities

due to its high organic carbon content that reaches up to 26.12 wt.% [7,11,13,14]. Earlier studies proposed that the Bilong Co oil shale bears similarities to asphalt-bearing shales that occur widely in the western Tethyan and Boreal realms, such as the Posidonia Shale in Germany [15]. The thick interval of the Quse oil shale in the Bilong Co section is thought to be deposited in response to the Toarcian Oceanic Anoxic Event (T-OAE) [6,9,16–18].

Oil shales are significant source rocks that play a crucial role in the generation and accumulation of hydrocarbons. They have been associated with significant perturbations in the global climate system and marine ecosystems throughout geological time [2,19–24]. To ensure accurate investigations of significant geological and biological events, particularly those pertaining to oil shales, an accurate geochronological framework is essential. However, the depositional age of the Bilong Co oil shale remains a subject of intense debate. Previous research on calcareous nannofossils suggested that the Bilong Co oil shale was deposited during the Middle Jurassic [25,26]. Although there is no report of age-diagnostic ammonites found in the Quse Formation to support a Toarcian age to date, Xia et al. conducted an analysis on palynomorph-rich assemblages of spores and dinoflagellate cysts [9], which revealed that the oil shale and the underlying limestone strata were deposited during the Toarcian (the late Early Jurassic). These conflicting viewpoints primarily arise from the controversial biostratigraphic chronology in the Bilong Co section. Moreover, the inclusion of the Bilong Co oil shale within the Early Jurassic Quse Formation is challenged by stratigraphic contacts and youngest detrital zircon ages [27]. Consequently, obtaining additional evidence of the bio-chronology and absolute age to establish an accurate geochronological framework in the Bilong Co section would greatly contribute to addressing key issues related to hydrocarbon exploration and the T-OAE. Such evidence, however, has not yet been reported.

In the western Tethys, biostratigraphic dating relies on high-resolution ammonite zones or subzones to precisely subdivide and resolve strata into biohorizons for Jurassic successions, particularly for those of the early Toarcian stage [28–31]. Therefore, in this study, six well-preserved ammonites were recovered for the first time from the uppermost part of the oil shales in the Bilong Co section to determine whether the Bilong Co oil shale was deposited during the Toarcian.

In addition, the lack of absolute ages remains a crucial factor contributing to the ongoing controversy surrounding the age of the Bilong Co oil shale. Syn-sedimentary volcanic beds are typically preferred for obtaining absolute geochronological ages of strata, but they are rare, especially in shales. Calcite is widely formed in various sedimentary environments. Calcite U–Pb dating could be a more widely applicable geochronometer if well-preserved carbonate mineral fractions can be dated with high precision [32–34]. It has been demonstrated that a reliable U–Pb dating age can be obtained from calcite using a Tera–Wasserburg inverse Concordia diagram [35–40]. In situ U–Pb dating technique (LA–MC–ICP–MS) has been successfully employed to determine the depositional age of calcite in carbonate sedimentary successions [40–49]. While calcite U–Pb dating cannot be directly used in shales, limestones interbedded within the shales are a choice for dating the main interval of the overlying shales. This approach may facilitate dating carbonate sedimentary successions that lack age-diagnostic fossils or syn-sedimentary volcanic beds. The ammonites, in combination with the calcite U–Pb age, should provide a more favorable means to constrain the stratigraphic age of the Bilong Co oil shale.

In this study, the emerging LA–MC–ICP–MS dating technique was applied, combined with newly obtained ammonite data from the Bilong Co oil shale. Thus, the objectives of this study are (1) to conduct in situ calcite LA–MC–ICP–MS U–Pb geochronology to determine the depositional history and age of the oil shale sediments in the Bilong Co section; and (2) to use age-diagnostic ammonites recovered from the upper part of the oil shale interval and provide relative age estimates together with in situ U–Pb ages to mutually validate one another. This not only allows for the determination of the depositional age of the Bilong Co oil shale but also provides a reliable time scale for the global comparison of

regional stratigraphy and the T-OAE (Toarcian Oceanic Anoxic Event) in the Qiangtang Basin (eastern Tethys).

### 2. Geologic Setting

The Qiangtang Basin is situated in the northern Tibetan Plateau, eastern Tethys, lying between the Hoh Xil–Jinshajiang suture zone and the Bangong–Nujiang suture zone [50] (Figure 1A). The Qiangtang Basin can be subdivided into the North Qiangtang Depression, the central uplift, and the South Qiangtang Depression [13,50] (Figure 1A). During the Permian to Late Triassic, the subduction of the Paleo-Tethys Oceanic crust beneath the Qiangtang terrane moved forward to the south, while the Hoh Xili terrane to the north led to the formation of a syn-tectonic foreland basin within the Hoh Xil–Jinshajiang suture zone [13,51]. Subsequently, an extensional tectonic system developed in the basin, marking the beginning of the Mesozoic Qiangtang Basin [12,50,52]. Jurassic marine deposits formed the most complete thick interval in the South Qiangtang depression, including the Lower Jurassic Quse Formation; the Middle Jurassic Sewa, Buqu, and Xiali formations; and the Upper Jurassic Suowa Formation [50] (Figure 2).

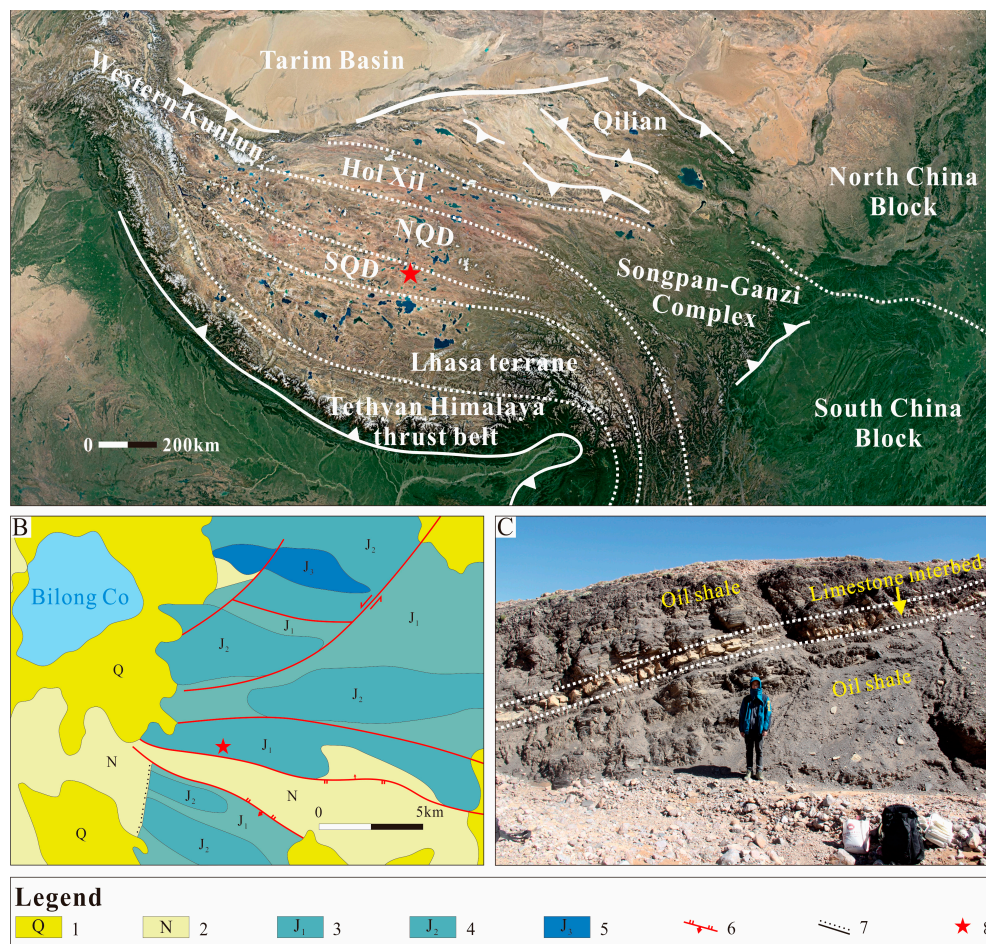


**Figure 1.** (A) Simplified topographic map of the Tibetan Plateau (modified from Google Earth Pro). (B) Geological map showing the major structural features and the location of the Bilong Co section (solid red star). (C) Field photograph of surface outcrop strata dominated by oil shale with limestone interbeds from the Bilong Co section. Note: 1-Quaternary, 2-Neogene, 3-Lower Jurassic Quse Formation, 4-Middle Jurassic Sewa, Buqu, and Xiali Formation, 5-Upper Jurassic Suowa Formation, 6-Fault, 7-Unconformity, 8-Study section in this study, NQD-North Qiangtang Depression, SQD-South Qiangtang Depression.

System	Series	Stage	Formation		Lithofacies	
Jurassic	Upper	Tithonian	Suowa		limestone, sandstone, siltstone	
		Kimmeridgian				
		Oxfordian				
	Middle	Callovian	Xiali		siltstone, sandstone, mudstone, gypsum	
		Bathonian	Buqu		limestone, marl	
		Bajocian	Sewa		marl, limestone, mudstone	
		Aalenian				
		Lower	Toarcian	Quse		oil shale, shale, limestone, marl, basalt, gypsum
	Pliensbachian					
	Sinemurian					
Hettangian						
Triassic	Upper	Rhaetian	Riganpei Co	Tumengela	mudstone, siltstone, limestone interbed	mudstone, siltstone, coal
		Norian				
		Carnian				

**Figure 2.** Schematic diagram showing the major lithostratigraphic units and lithofacies composition of the Upper Triassic–Jurassic in the South Qiangtang Depression [50].

The Quse Formation in the Bilong Co section is characterized by a combination of shales containing abundant ammonoids and bivalves intercalated with thin-bedded limestones (Figure 1B,C). These facies have been interpreted as deposits formed in a shallow sea within a semi-restricted marginal marine basin [6,53]. Notably, significant negative carbon-isotope excursions (N-CIEs) of about 3‰ have been reported in the oil shale interval of the Bilong Co section [6,9,18,54]. However, chronological evidence to ascertain the correlation with the T-OAE is still a matter of significant debate. Therefore, this study focuses on the chronology of the oil shale interval of the Bilong Co section, which roughly matches the 5–40 m interval of the succession previously reported by Fu et al. [6] (Figure 1C). This oil shale interval is characterized by millimeter-laminated beds of 0.2–2.0 cm thick black and dark gray shales interbedded with light gray to white limestone (Figure 1C).

### 3. Material and Methods

#### 3.1. Samples

The current study Bilong Co section was collected from the Bilong Co area at longitude 88°54′28.32″ E and latitude 32°49′56.58″ N. Three carbonate specimens were collected from the limestone interbed within the Bilong Co oil shale (Figure 3). One of them was chosen carbonate LA–MC–ICP–MS U–Pb geochronological analysis (Figure 4), while three samples (including a U–Pb sample) were selected for element analyses. Additionally, six ammonite fossils were collected from gray shales at the uppermost part of the Bilong Co oil shale section for species identification (Figure 5).

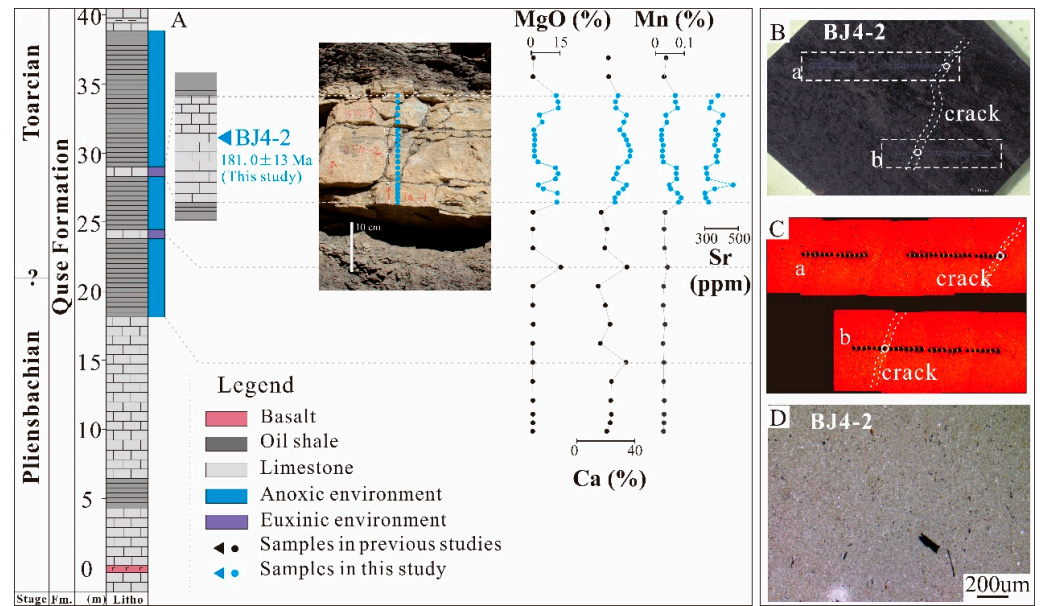


**Figure 3.** Vertical variations of diagenesis proxies (MgO, Ca, Mn, and Sr) and micrographs of limestone sample BJ4-2. (A) Geochemical data measured by Hand-Held X-ray fluorescence (HH-XRF). Blue circles are data in this study. Black circles refer to data measured by Fu et al. [6]. (B,C) Reflected light (LIBS) and CL images showing weak diagenesis and highlighting the regions analyzed for U–Pb. CL images are almost dark to the naked eye, and thus the brightness is turned up by a fixed amount to show the textural detail. The white dotted lines highlight the cracks caused during sample preparation, and thus the spots in white circles were excluded from the calculation of calcite U–Pb ages. (D) Limestone interbed mainly consists of microspar showing weak diagenesis under the plane polarized light.

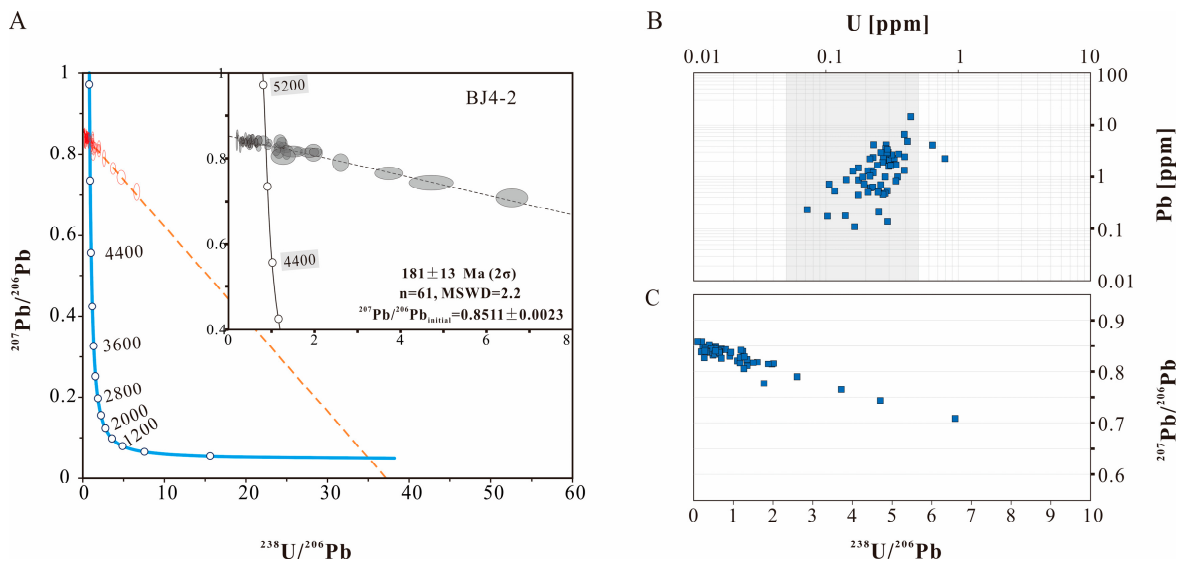


**Figure 4.** In situ calcite U–Pb isotopic analysis of the limestone sample BJ4-2. (A): Shows a cross-plot of  $^{238}\text{U}/^{206}\text{Pb}$  versus  $^{207}\text{Pb}/^{206}\text{Pb}$  Tera–Wasserburg Concordia diagrams. Gray dashed line represents the isochrons. Ellipses represent the ‘n’ spot analyses and corresponding isotope ratios obtained. Solid black line represents the Concordia curves. All ages are reported with  $2\sigma$  confidence. (B): Cross-plot of Uranium (U) versus Lead (Pb) concentrations expressed in parts per million (ppm). (C): Cross-plot of  $^{238}\text{U}/^{206}\text{Pb}$  versus  $^{207}\text{Pb}/^{206}\text{Pb}$  ratios showing a wide range in sample BJ4-2.

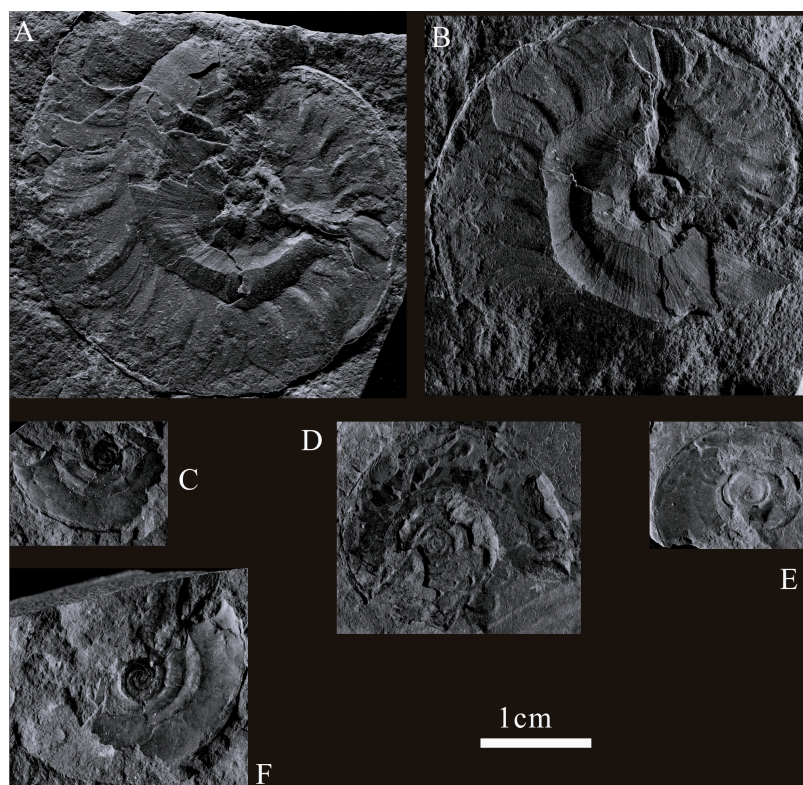


**Figure 5.** Photographs of ammonites recovered from the Bilong Co section. (A,B,E): *Tiltoniceras* sp., late Pliensbachian–early Toarcian recovered from samples JJ-01, JJ-02, and JJ-05, respectively. (C,D,F): *Hildoceratidae* sp., Early Jurassic, taken from samples JJ-03, JJ-04, and JJ-06, respectively.

### 3.2. Petrography and Palaeontology

Thin sections with a thickness of 40  $\mu\text{m}$  were meticulously prepared to differentiate various mineral components. Ammonite classification followed the methodology established by Howarth et al. [55]. Conventional optical petrography was conducted using a Lecia DM750P polarized light microscope and a Nexcope NSZ818 stereomicroscope under plane- and cross-polarized light. The species identification of ammonites was carried out at the Nanjing Institute of Geology and Palaeontology, Chinese Academy of Sciences (NIGP-CAS). Cathodoluminescence (CL) imaging was performed using a Canada BII-CLF2 cold cathode apparatus mounted on a Lecia DM750P microscope, utilizing a beam with voltages ranging from 10 to 15 kV and currents ranging from 400 to 500 mA.

### 3.3. LA–MC–ICP–MS U–Pb Isotope Analyses

In situ U–Pb dating was conducted at the Key Laboratory of Carbonate Reservoir of China National Petroleum Corporation (CNPC). Before U–Pb LA–MC–ICP–MS dating, optical examination (including microscopy and cathodoluminescence imaging) and geochemical diagenetic analyses were conducted to distinguish areas of alteration. Afterwards, a polished epoxy-impregnated rock chip mount was cleaned in an ultrasonic bath with ethanol, and the entire system was flushed with helium gas. In situ U–Pb isotopic analysis was conducted on the sample, following a procedure similar to that described in Nuriel et al. [56] and Shen et al. [57]. During the analysis, a manual pre-screening session allowed the identification of areas with variable U/Pb and  $^{207}\text{Pb}/^{206}\text{Pb}$  ratios. Then, samples were ablated in a helium atmosphere. The ablation used a 120- $\mu\text{m}$ -square spot at a laser repetition rate of 10 Hz and a laser energy of 3 J/cm<sup>2</sup>. The NIST 614 glass standard was used as the primary reference material to correct for the  $^{207}\text{Pb}/^{206}\text{Pb}$  ratios of the carbonate reference materials and unknowns and instrument drift in the  $^{238}\text{U}/^{206}\text{Pb}$  ratio. The  $^{238}\text{U}/^{206}\text{Pb}$  ratios of calcite samples were further calibrated with calcite standards, the ID-MS calibrated

calcite standards Damy (221.0 ± 4.6 Ma) [58] and AHX-1 (209.8 ± 1.3 Ma) [59], following the method described in Roberts et al. [58] and Shen et al. [57]. The sample age was regressed on Tera–Wasserburg plots using Isoplot 3.0 [60] after raw data were processed by Iolite 3.6. Then, the age was verified and recalculated for initial 207Pb/206Pb by the online IsoplotR program [61]. All uncertainties are reported as 2σ.

### 3.4. Element Analyses

All sediment samples were air-dried, sieved, and crushed into fine fractions of 200 μm size before analysis. Each X-ray fluorescence (XRF) sample cup was filled with approximately 7 g of sediment (dry weight) until full, after which the cup was sealed with ultralene film. The Hand-Held (HH) Bruker S1 Titan XRF Alloy Analyzer (Billerica, MA, USA) was used to screen the samples at the Southwest Petroleum University. The instrument comprises an X-ray tube with a Rhodium (Rh) anode (4 W, 15–50 kV, 5–100 μA) and a Silicon Drift Detector (FAST SDD) with a resolution of <145 eV, based on the Peltier Effect. Check-sample Bruker® was utilized for quality assurance and quality control, with recoveries (%) of elements ranging between 90 and 100. The HH-XRF has a detection limit of less than 0.5 g kg<sup>-1</sup>.

## 4. Results

### 4.1. Ammonites

A total of six ammonite specimens were recovered from the Bilong Co section. Two species (Figure 5), containing *Hildoceratidae* sp. and *Tiltoniceras* sp., were identified at the NIGP-CAS. In this study, in situ ammonites of the *Hildoceratidae* family, containing *Tiltoniceras* sp. (Figure 5), were collected from gray marls at the top of Interval III (see Figure 5). The importance and stratigraphic significance of the recorded age diagnostic marker ammonites will be discussed in Section 5.1.

### 4.2. U–Pb Geochronology

The concentrations and isotope ratios of U and Pb in the analyzed samples are summarized in Figure 4B. The U concentrations of sample BJ4-2 range from 0.07 to 0.8 ppm, exhibiting variability in the <sup>238</sup>U/<sup>206</sup>Pb ratios, which ranges from 0.1 to 6.6 (Figure 4C). Tera–Wasserburg Concordia plots displaying lower intercept ages can be found in Figure 4A. The complete data set and plots can be found in the Supplementary Materials.

Sample BJ4-2 originates from the limestone interbed within the oil shales (Figures 3 and 6). A total of 63 spot analyses were conducted on microspar in sample BJ4-2 (Figure 4). Two spot analyses on a crack (which was generated during sample preparation) were excluded for calcite U–Pb dating (Figures 3B and 4C), resulting in 61 spot analyses being utilized to determine the U–Pb age of the BJ4-2 sample. Some of the data have low radiogenic Pb and anchor the extrapolation to a lower intercept Concordia date with a relatively high radiogenic Pb content, but the small-scale isochron yields a realistic intercept age.

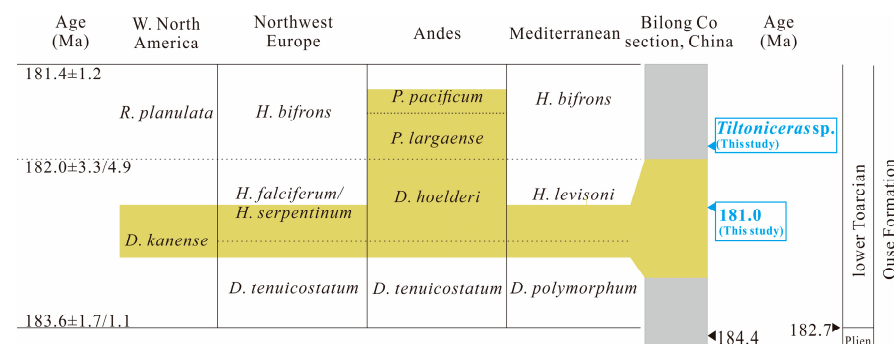


**Figure 6.** Regional ammonite biostratigraphic correlation from Western North America, Northwest Europe, Andes, and Mediterranean [62,63], and absolute U–Pb age data [64,65] during the early Toarcian.

### 4.3. Elemental Geochemistry

The Sr contents in the carbonate exhibit relatively high values from the bottom to the top of the limestone interbed, ranging from 305 to 469 ppm. The Mn/Sr ratios of the carbonate samples from the middle part of the limestone interbed (spots 9–17) are consistently below 2, and generally below 5 in the lower and upper part (spots 1–8 and 18–20) (Figure 3A). The Mg/Ca ratios are consistently below 0.6 throughout the entire limestone interbed, and usually below 0.1 in the middle part (Figure 3A).

## 5. Discussion

### 5.1. Age Constraints Based on Bio-Chronological Data

Since the stratigraphic columns reported in the Bilong Co section and adjacent areas commonly vary, a clear stratigraphic correlation is necessary to constrain the intervals in which age-diagnostic fossils occur before discussing the biostratigraphy of the current study Bilong Co section (Figure 6). Based on the lithological and geochemical features, the Bilong Co section can be divided into four intervals (Figure 7): Interval I, marked by a basalt interbed that can be used as a marker event to enhance the lithostratigraphic correlation of other marls and limestones between the lithologic column c [9] and lithologic column d [6] (Figure 7); Interval II, a thick oil shale bed (excluding oil shale interbeds) that is characterized by N-CIEs, can further serve as a marker for stratigraphic correlations; Interval III, made up of gray shales (with minor oil shale interbeds) interbedded by limestones and characterized by the end of N-CIEs. Interval IV occurs at the upper part of the Bilong Co section, and consists mainly of intercalations between mudstone, calcareous mudstones, and marls.

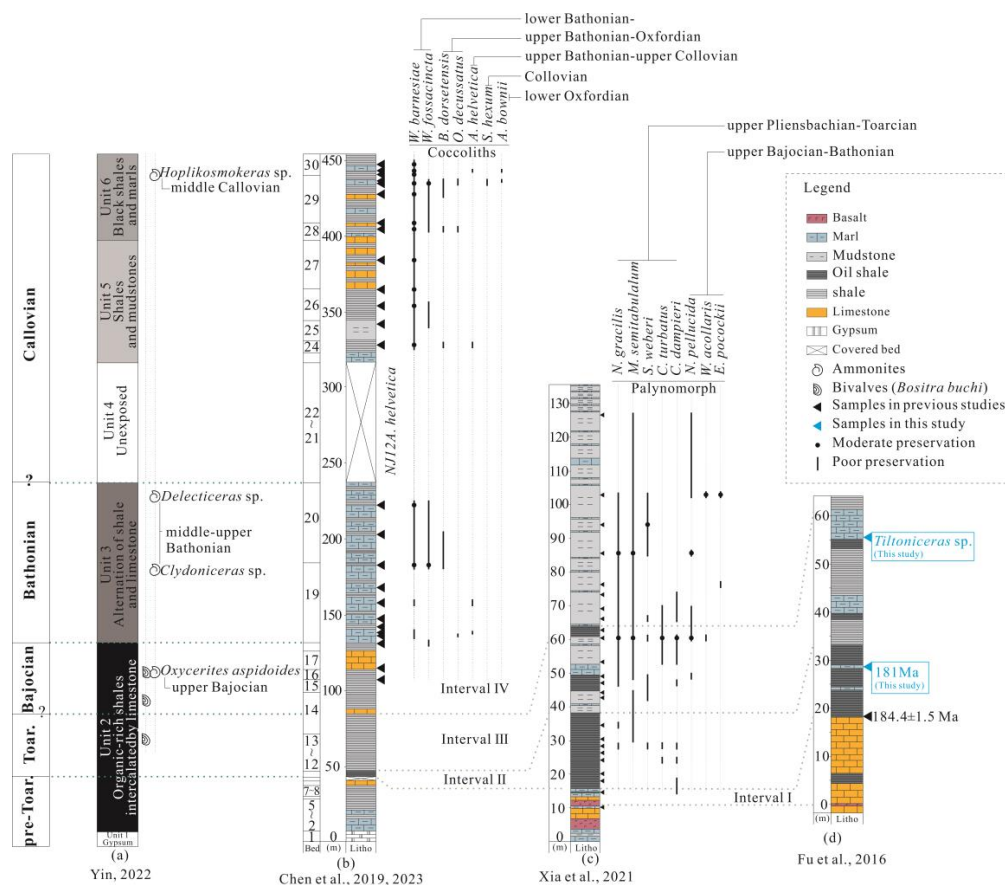


**Figure 7.** Comprehensive regional biostratigraphic and lithostratigraphic correlation of the Bilong Co oil shale, showing that no calcareous nannofossils and ammonoid constraints occur in the lower Quse Formation [53]. Proposed ages and data source are from (a)-[26], (b)-[25,66], (c)-[9], (d)-[6].

In the Bilong Co section, the marker coccoliths species *Ansulaspheera helvetica* defines the nannofossil NJ12 Zone, which corresponds to a late Bathonian to Callovian age [25]. Moreover, the ammonite species *Oxycerites aspidoides* is indicative of a late Bajocian age, whereas *Clydoniceras discuss* defines a late Bathonian age, both of which were reported in beds 16 and 20 (Figure 7, section a), respectively [26], corresponding to ~110 m and ~200 m in the Bilong Co section of Chen et al. [25] (Figure 7, section b). The occurrence of bivalve species *Bositra buchi* is reported in beds 3–18 in the Bilong Co section of Yin [26] (Figure 7, section a). However, these bivalves have a long age range. Obviously, stratigraphic correlations indicate that age-diagnostic ammonites and bivalves of Yin [26] and coccoliths of Chen et al. [25] should be placed in Interval IV or higher. Their presence along with marine microplanktons, mainly of dinoflagellate cysts *Nannoceratopsis pellucida*, *Wanaea acollaris*, and *Escharisphaeridia pocockii* [9], indicates that sediments of Interval IV were deposited during the Bajocian–Bathonian (Figure 7). Bajocian ammonites *Dorsetensia* sp. and *Witchellia* sp. suggest a Bajocian age for the Sewa Formation [67–69], while Bathonian brachiopods *Burmihynchia–Holcothyris* from the conformably overlying Buqu Formation [52] reveal that the Sewa Formation was deposited no later than the Bathonian. Therefore, the lower part of Interval IV is considered to belong to the Sewa Formation. However, there are no age-diagnostic ammonites and coccoliths recorded in Intervals I–III, within which sediments should be deposited earlier than the Bajocian. It is worth noting that Yin mentioned a nannofossil record and proposed a middle Toarcian–Aalenian age for the bed 1–8 in the stratigraphic column b [26] (Figure 7), but only poorly preserved or long-ranging species were identified between 0–100 m as Chen et al. [66] suggested (Figure 6). Hence, the nannofossil mentioned above should be re-examined to ensure that it can be placed at the correct interval of the Bilong Co section.

The Hildoceratidae is one of the ammonite families that dominates the lower Toarcian British strata [55]. *Tiltoniceras* is typically known to have an appearance that is exclusive to the Early Jurassic and ranges from the late Pliensbachian to early Toarcian [55]. *Tiltoniceras* originated during the late Pliensbachian epoch in the northern Pacific [70], and it frequently occurred in the *Tenuicostatum* Zone (lower Toarcian) in the Tethyan Realm and became abundantly recorded in the *Exaratum* Subzone [17,55]. This genus is prevalent and well-preserved in the *Tenuicostatum* Zone in NE Siberia [55]. In western North America, the base of the *Kanense* Zone corresponds to the beginning of the Toarcian period, and *Tiltoniceras* extended into the *Kanense* Zone and disappeared above *Dactylioceras kanense* [71]. *Tiltoniceras* is usually found alongside *Dactylioceras* and has been reported in Toarcian strata from the Westgate District of central Nevada [70], southern Yukon Territory [71], and Nechako River map area [71]. The presence of in situ *Tiltoniceras* sp. attests that the oil shales in the Bilong Co section can be consistent with the top of the *Tenuicostatum* Zone in Europe and the lower *Kanense* Zone in western North America (Figure 6), providing an early Toarcian age for the Bilong Co oil shale. In addition, Xia et al. [9] recovered a rich assemblage of dinoflagellate cysts from the Bilong Co section (Figure 7), indicative of an early Toarcian age. This includes *Nannoceratopsis gracilis*, *Mancodinium semitabulatum*, *Scrinioicassis priscus*, and *Scrinioicassis weberi*, which were identified from Interval II to IV. This dinoflagellate cyst assemblage is commonly recorded within the upper Pliensbachian to lower Toarcian strata from the Tethyan Realm in the UK and NW Scotland, central Italy, and western Portugal [72,73]. Other age-diagnostic palynomorphs were reported from the Quse Formation in the Bilong Co section, such as pollen grain species *Callialasporites trilobatus*, *Callialasporites dampieri*, and *Callialasporites microvelatus*, which spur further evidence of the Toarcian [9]. Long-ranging pollen grains, such as *Classopollis* sp., *Spheripollenites psilatus*, and *Corolina torosa*, are characteristic features of the latest Pliensbachian–Toarcian in the Bilong Co section, Qiangtang Basin [9], the Ordos Basin, North China [74], NW Scotland [72], and the Lusitanian Basin, western Portugal [73]. Thus, recurrent occurrences of these age-diagnostic dinoflagellate cyst and pollen grain species in Intervals II to IV further support an early Toarcian age constraint of in situ ammonites in the Bilong Co oil

shale section. Therefore, the Bilong Co oil shale strata should belong to the Early Jurassic Quse Formation (Figure 7).

## 5.2. Calcite U–Pb Geochronology

### 5.2.1. Primary Depositional Age

Interpretations of calcite U–Pb ages are based on the amounts of radiogenic U and Pb and uncertainties of ablation points in the collected carbonate samples, although the complex variability of these data makes this task challenging. Two objective criteria were followed to help select reliable ages. Owing to the limitation of small-sample statistics for most geochronological data sets, a cutoff of less than 2.5 is suggested, and the data for which Mean Squared Weighted Deviation (MSWD) are more than 2.5 reflect calculated ages with dubious geologic significance [75]. Additionally, age uncertainties of less than 10% are required for robust ages [43]. Here, sample BJ4-2 provides an age estimate of  $181 \pm 13$  Ma with MSWD 2.2, which is below the threshold line of 2.5 (Figure 4A).

Calcite can be formed in both syn- and post-depositional (diagenetic) stages. If the U–Pb isotopic system of calcite is altered by late diagenesis, the dating ages may not represent the primary depositional age of the calcite [36,37]. The potential diagenesis of the Quse Formation (including limestone interbeds) in the Bilong Co section has been examined through geochemical studies. Earlier investigations of the Bilong Co section concluded that diagenesis has a negligible effect on the original isotopic signals of bulk carbonate and organic carbon present in the studied limestone bed [6]. In this study, additional detailed work was conducted on the limestone interbed, including microscopic and geochemical studies to provide further evidence of the depositional history of the Bilong Co oil shale section (Figure 3). Sample BJ4-2 consists mainly of microspar, and microscopic observation shows that it has not been significantly altered by diagenesis, except for dissolution and dolomitization in the BJ4-1 and BJ4-3 intervals (Figure 3D). Dated regions are also far from veins, laminations, and other textural heterogeneities (Figures 3B and 4C). The Mg/Ca ratio is often used to indicate the degree of dolomitization [76,77]. Most of the ratios in the BJ4-2 interval of the limestone interbed are less than 0.1, probably reflecting the stability of the primary isotope system (Figure 3A). Mn/Sr ratios are typically less than 2; thus, the BJ4-2 interval may not have been altered by post-depositional fluid flow [65,78]. Since strontium is easily lost during water–rock interaction, Sr concentration data are highly sensitive to minimal levels of the interaction, encompassing nearly all diagenetic pathways [77]. The BJ4-2 interval typically has Sr concentrations exceeding 300 ppm and Mn concentrations below 500 ppm (Figure 3A), suggesting that these values are typical of little-altered marine compositions [77]. Even areas with elevated Sr concentration (305–469 ppm) can have Mn/Sr ratios up to 4.6 in spots of the BJ4-1 and BJ4-3 intervals. It is worth noting that these two samples directly interface with the oil shales, while elevated Mn/Sr ratios are often interpreted as post-depositional alteration. It is suggested that these ratios from these spots indicate limited post-depositional alteration. Based on the Mg/Ca ratio of less than 0.6 and Sr concentration of higher than 300 ppm within the BJ4 interval, the moderate increase in Mn/Sr ratios is interpreted to reflect carbonate deposition from anoxic marine fluids. Since the age was derived from the calcite that composes the sample, the estimated age of  $181 \pm 13$  Ma is interpreted as the primary depositional age of the limestone interbed, which is also supported by the relatively good preservation of carbonates in the Bilong Co oil shale.

### 5.2.2. Age Assessment Based on Radioisotopic Dates

Due to the relatively well-preserved carbonates in the Bilong Co section, it is proposed that the calcite U–Pb age of  $181 \pm 13$  Ma can be considered as the primary age of the sampled horizon. The Toarcian stage represents the final phase of the Early Jurassic, spanning from *ca.* 182.7 to *ca.* 174.1 Ma [79]. The age of *ca.* 181 Ma, near the base of the Toarcian, can be regarded as an early Toarcian age, which is supported by the recorded fossil groups (Figure 6). Regional correlation of ammonite zones suggests that the combined

*Tenuicostatum* and *Falciferum* zones in NW Europe are approximately simultaneous with the *Kanense* Zone in North America [63,71] (Figure 6). U–Pb ages obtained from the Toarcian strata in North America indicate that the duration of the T-OAE is constrained within a narrow range, from  $183.6 \pm 1.7/1.1$  Ma to  $182.0 \pm 3.3/4.9$  Ma (zircon ICP-MS U–Pb) [64,80,81]. The new calcite U–Pb age (*ca.*  $181 \pm 13$  Ma, calcite LA-ICP-MS U–Pb) obtained in this study overlaps with this range, despite the uncertainty of the measured age range. This suggests a good agreement not only with global Toarcian ammonite zones but also with worldwide chronostratigraphic assessments based on radioisotopic ages during the T-OAE. At the same time, the proposed radioisotopic age also fits exactly with constraints of the regional chronostratigraphy. The youngest age of detrital zircons peak at  $184.4 \pm 0.61$  Ma (zircon LA-ICP-MS U–Pb) has been given from the base of the Bilong Co oil shale [6], suggesting a maximum depositional age of this oil shale interval not younger than Toarcian. Additionally, this interval was previously interpreted under enhanced oxygen-deprived bottom water conditions and an N-CIE, consistent with a record of the T-OAE in this part of the eastern Tethys [6,7,9,53]. Ma et al. [82] obtained a maximum deposition age for the Sewa Formation between  $175.9 \pm 3$  Ma and  $171.7 \pm 5.1$  Ma (zircon LA-ICP-MS U–Pb), implying an upper Toarcian–lower Aalenian age. Thus, the interpreted calcite U–Pb age date of 181 Ma for the Bilong Co oil shale in this study falls within the known radioisotopic age constraints of  $184.4 \pm 0.61$  Ma to  $171.7 \pm 5.1$  Ma.

In conclusion, although the uncertainty range of  $\pm 13$  Ma allows for an age assignment ranging from the Early Jurassic into the Middle Jurassic, it is suggested that the Bilong Co oil shale was likely deposited around *ca.* 181 Ma, supported by in situ ammonites and radioisotopic dates, thus providing a new absolute chronological marker for the Bilong Co section.

### 5.3. Significance of the New Geochronology in the Bilong Co Section

To ensure reliable investigations of voluminous geological and biological events and the evaluation of hydrocarbon resources, particularly for oil shales, it is essential to establish an accurate geochronologic framework. In this study, data from sedimentary successions, geochemistry, and chronology are integrated to reconstruct a comprehensive chronostratigraphic framework of the Jurassic period in the Bilong Co area (Figure 7). Additionally, the source-reservoir-seal system in the South Qiangtang Depression will be discussed.

## Reconstruction of the Chronostratigraphic Framework in the Bilong Co Section

### Pre-Toarcian

This stage corresponds to Interval I, which is constrained by a basalt age of *ca.*  $201.8 \pm 0.45$  Ma at the base and a youngest detrital zircon peak of *ca.*  $184.4 \pm 0.61$  Ma at the top [6]. Sediments overlying the basalt interbed consist mainly of limestone with a few shale beds, resembling the biotic carbonate platforms that were widespread in the western Tethys [83–86]. These sediments are attributed to the lower part of the Quse Formation [7].

### Toarcian

This stage corresponds to lithologic Intervals II and III, constrained by in situ U–Pb dating of *ca.* 181 Ma and the Toarcian marker ammonites *Tiltoniceras* sp. recovered at the top. At this time, the demise of the biotic carbonate platform led to the predominance of water column bioproductivity and regional accumulation of a thick interval of oil shales [86]. These sediments are featured by N-CIEs that are characteristic of the T-OAE throughout the Tethys [6,9,54].

### Aalenian

Ammonites reported south of the Angda'er Co area reveal that the upper part of the Quse Formation may extend into the Aalenian [82]. Furthermore, the presence of the ammonite species *Planammatoceras* cf. *lepsiusi* and *Phylloceras* sp. in the Exiubu section suggests that gray shales and mudstones overlying Toarcian black shales were deposited during the Aalenian [26,87]. Although no age-diagnostic fossils or absolute ages implying

an Aalenian age were found in the Bilong Co section, it is inferred, based on stratigraphic contacts, that the base of Interval IV represents the Bajocian sediments.

#### Bajocian

This stage corresponds to the lower part of Interval IV. The boundary between the Bajocian and the Bathonian can be constrained based on the ammonite *Oxycerites aspidoides* and bivalve *Bositra buchi* assemblage, indicative of a late Bajocian age [26]. The age-diagnostic calcareous nannofossils species *Watznaueria barnesiae* and *Watznaueria fossacincta* are indicative of an early Bathonian age [25] (Figure 7). Sediments during this period consist mainly of marls and mudstones with minor limestone interbeds, which are attributed to the Sewa Formation.

#### Bathonian

This stage should correspond to the lower part of Interval IV, and the occurrence of the Bathonian ammonites were reported [26] (Figure 7). Due to limited exposure, the boundary between the Bathonian and the Callovian remains unclear. Sediments during this interval consist of shallow-water limestones, which may suggest the re-development and recovery of biotic platforms along the entire Tethyan margin after the T-OAE. Based on the lithologic composition and bio-chronology, these sediments should belong to the Buqu Formation. The unexposed interval is likely the Xiali Formation, which conformably overlies the Buqu Formation based on stratigraphic contacts [13].

#### Callovian

This stage corresponds to the upper part of Interval IV and consists of limestones and shales, yielding middle Callovian ammonites *Hoplikosmokeras* sp. [26]. Sediments during this period are assigned to the Suowa Formation based on petrology and bio-chronology [13,26].

#### 5.4. Regional Chemostratigraphic Correlation and Implication for the Quse Oil Shale Age

Regional correlation of carbon isotope excursion events can provide indirect, yet important inferences of the timing of the carbon cycle major perturbations and related oceanic anoxic events. Recent investigations of regional to global carbon isotope correlation revealed that the T-OAE is characterized by highly variable magnitudes of N-CIE from  $-0.8\%$  to  $-8.6\%$  [2]. Within the Quse Formation, high-resolution carbon isotopes of organic matter ( $\delta^{13}\text{C}_{\text{org}}$ ) [6] and kerogen ( $\delta^{13}\text{C}_{\text{kerogen}}$ ) [9] have been measured (Figure 8). The lower Toarcian oil shales of the Quse Formation showed an abrupt N-CIE with a maximum magnitude of  $\delta^{13}\text{C}_{\text{kerogen}}$  at  $5.23\%$  and  $3\%$  on average [9] (Figure 8), consistent with the early Toarcian carbon cycle perturbation associated with the T-OAE. This is in agreement with  $\delta^{13}\text{C}_{\text{org}}$  values from the same interval in the Bilong Co area with a N-CIE average magnitude of  $2.8\%$  [6] (Figure 5). The Quse N-CIE exhibits a comparable pattern with other regional sections from China, such as the Niandua and Wölong sections from the Tibetan Himalaya [86], the Anya section in the Ordos Basin [74], and the Suobucha section in the Southern Qiangtang Depression (Figure 8). Therefore, the N-CIE of the Quse Formation in the Bilong Co area can commonly refer to the onset of the lower Toarcian oil shale deposition. Additionally, the N-CIE of the Quse oil shale is comparable to the coeval range from well-preserved T-OAE intervals in the western Tethys, including the Yorkshire section in the UK [4,88], the Peniche section in the Lusitanian Basin in Portugal [1,31], and the Riethem Posidonia Shale in northern Switzerland [5], providing evidence of the Quse oil shale depositional age during the Toarcian. It is therefore concluded that  $\delta^{13}\text{C}_{\text{kerogen}}$  and  $\delta^{13}\text{C}_{\text{org}}$  excursions are an expression of the early Toarcian global carbon perturbation, which assign a Toarcian age to the Bilong Co oil shales that is compatible with coeval records sections in the eastern Tethys, as well as with far-apart sections worldwide.

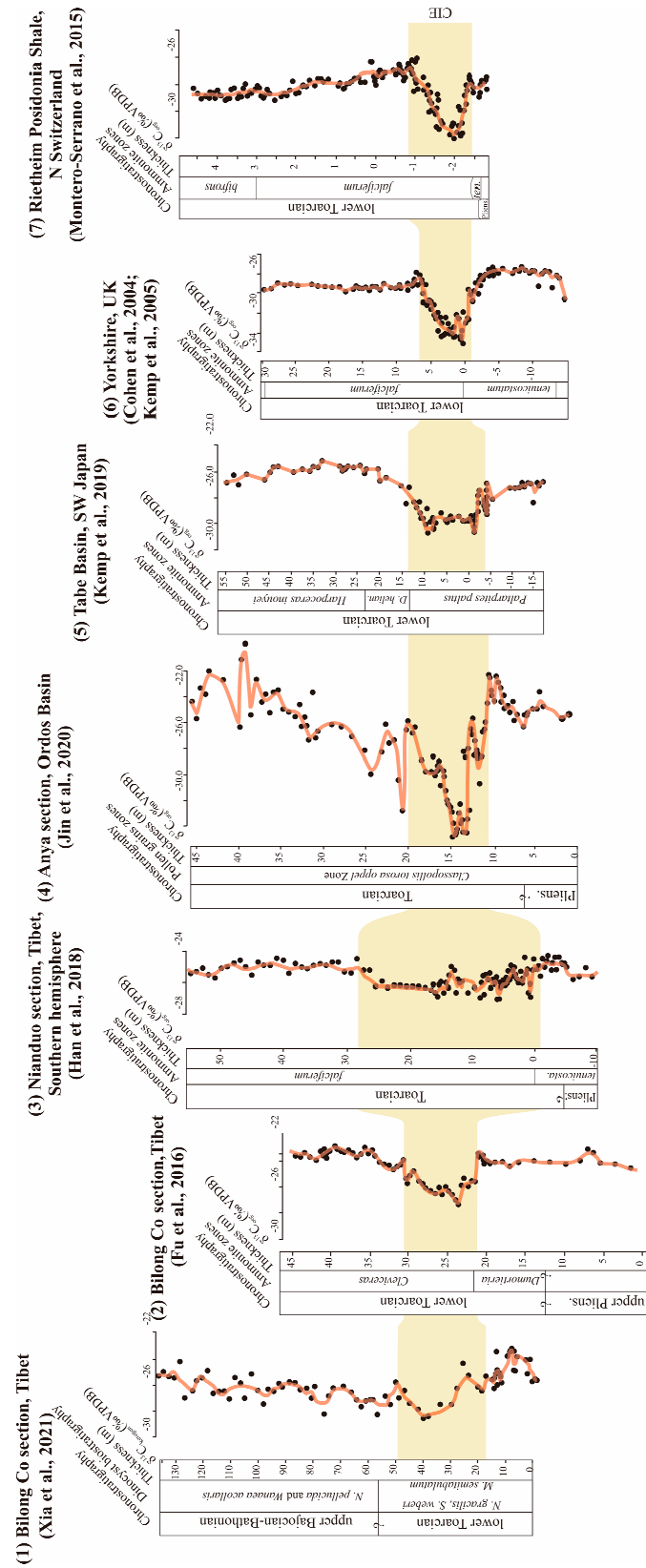


**Figure 8.** Regional correlation of carbon isotope profiles of kerogen [54], organic matter [6,9], and bulk carbonate [6], showing the negative excursion that characterizes the Toarcian oceanic anoxic event from the eastern Tethys (southern Tibet and Tibetan Himalaya in southern hemisphere) [86], Panthalassa Ocean (southwest Japan) [89], and northwestern Tethys (the UK [4,88] and northern Switzerland [5]).

## 6. Conclusions

Based on an integrated approach of in situ carbonate U–Pb dating and invertebrate micropalaeontology, mainly of marker ammonites, from the Bilong Co oil shale section along with regional correlation from coeval stratigraphic sections in the Qiangtang Basin, the following conclusions are developed.

- (1) The previous investigations of age estimates are supported by the new in situ carbonate U–Pb isotope dating, suggesting that the Quse oil shale in the Bilong Co area was deposited during the Early Jurassic.
- (2) Newly discovered age-diagnostic ammonite assemblage revealed that the age constraint for the Bilong Co oil shale is the early Toarcian, rather than the previous suggestions of a Middle Jurassic age.
- (3) Regional correlation of in situ carbonate U–Pb isotope dating along with marker ammonites, bivalves, and calcareous nannofossils from adjoining sedimentary sections in the Bilong Co area provide further evidence of an early Toarcian age of the oil shale strata.
- (4) New geochronologic results and regional correlation of N-CIE indicate that the Quse oil shale provides a record of the global T-OAE in the eastern Tethys generally and the Qiangtang Basin particularly. This result provides new significance of further regional evaluation of source rocks in the Qiangtang Basin.

**Supplementary Materials:** The following supporting information can be downloaded at: <https://www.mdpi.com/article/10.3390/min14030246/s1>.

**Author Contributions:** Conceptualization: J.W.; methodology: J.W.; validation: H.Z.; formal analysis: H.Z., J.Z., H.W., X.F., L.S. and S.X.; investigation: H.Z., H.W. and X.F.; data curation: H.Z., H.W.; writing—original draft preparation: H.Z. and A.M.; writing—review and editing: A.M., M.S.A. and T.G.; visualization: H.Z.; supervision: J.W.; project administration: H.Z. and J.W. All authors have read and agreed to the published version of the manuscript.

**Funding:** This work was supported by the National Natural Science Foundation of China (Grant No. 42241202), the Second Tibetan Plateau Scientific Expedition and Research Program (STEP) (Grant No. 2019QZKK080301), the National Natural Science Foundation of China (42241203), the Researchers Supporting project number (RSP2024R455), King Saud University, Riyadh, Saudi Arabia, and the 14th Five-Year Prospective and Basic Research Project of Petro China (2021DJ0801).

**Data Availability Statement:** The data presented in this study are openly available at [www.mdpi.com/xxx/s1](http://www.mdpi.com/xxx/s1).

**Acknowledgments:** We are thankful to Anjiang Shen, Anping Hu, and Feng Liang for their support during experiments. We are also indebted to Zhongwei Wang for detailed discussions and the improvement of the manuscript. We are thankful to the Minerals editorial board and to the three anonymous reviewers for their valuable and constructive comments.

**Conflicts of Interest:** Thomas Gentzis was employed by Core Laboratories. The remaining authors declare that the research was conducted in the absence of any commercial or financial relationships that could be construed as a potential conflict of interest.

## References

1. Hesselbo, S.P.; Jenkyns, H.C.; Duarte, L.V.; Oliveira, L.C.V. Carbon-isotope record of the Early Jurassic (Toarcian) Oceanic Anoxic Event from fossil wood and marine carbonate (Lusitanian Basin, Portugal). *Earth Planet. Sci. Lett.* **2007**, *253*, 455–470. [[CrossRef](#)]
2. Remírez, M.N.; Algeo, T.J. Carbon-cycle changes during the Toarcian (Early Jurassic) and implications for regional versus global drivers of the Toarcian oceanic anoxic event. *Earth-Sci. Rev.* **2020**, *209*, 103283. [[CrossRef](#)]
3. Ruebsam, W.; Pińkowski, G.; Schwark, L. Toarcian climate and carbon cycle perturbations—Its impact on sea-level changes, enhanced mobilization and oxidation of fossil organic matter. *Earth Planet. Sci. Lett.* **2020**, *546*, 116417. [[CrossRef](#)]
4. Cohen, A.S.; Coe, A.L.; Harding, S.M.; Schwark, L. Osmium isotope evidence for the regulation of atmospheric CO<sub>2</sub> by continental weathering. *Geology* **2004**, *32*, 157–160. [[CrossRef](#)]

5. Montero-Serrano, J.-C.; Föllmi, K.B.; Adatte, T.; Spangenberg, J.E.; Tribouillard, N.; Fantasia, A.; Suan, G. Continental weathering and redox conditions during the early Toarcian Oceanic Anoxic Event in the northwestern Tethys: Insight from the Posidonia Shale section in the Swiss Jura Mountains. *Palaeogeogr. Palaeoclimatol. Palaeoecol.* **2015**, *429*, 83–99. [[CrossRef](#)]
6. Fu, X.G.; Wang, J.; Feng, X.L.; Wang, D.; Chen, W.B.; Song, C.Y.; Zeng, S.Q. Early Jurassic carbon-isotope excursion in the Qiangtang Basin (Tibet), the eastern Tethys: Implications for the Toarcian Oceanic anoxic event. *Chem. Geol.* **2016**, *442*, 62–72. [[CrossRef](#)]
7. Xia, G.Q.; Mansour, A. Paleoenvironmental changes during the early Toarcian Oceanic Anoxic Event: Insights into organic carbon distribution and controlling mechanisms in the eastern Tethys. *J. Asian Earth Sci.* **2022**, *237*, 105344. [[CrossRef](#)]
8. Ruebsam, W.; Al-Husseini, M. Orbitally synchronized late Pliensbachian–early Toarcian carbon-isotope and glacio-eustatic cycles. *Palaeogeogr. Palaeoclimatol. Palaeoecol.* **2021**, *577*, 110562. [[CrossRef](#)]
9. Xia, G.Q.; Mansour, A.; Gentzis, T.; Li, G.J.; Carvajal-Ortiz, H.; Ocubalidet, S.; Yi, F.; Yun, C.; Yi, H.S. Depositional paleoenvironment and source rock characterization across the Toarcian Oceanic Anoxic Event from the eastern Tethys, Tibet, SW China. *Int. J. Coal Geol.* **2021**, *243*, 103780. [[CrossRef](#)]
10. Zhao, Z.Z.; Li, Y.T.; Ye, H.F.; Zhang, Y.W. *Tectonic Characteristics and Basin Evolution of the Tibetan Plateau*; Science Press: Beijing, China, 2001; pp. 93–97. (In Chinese with English Abstract)
11. Wang, J.; Tan, F.W.; Li, Y.L.; Li, Y.T.; Chen, M.; Wang, C.S.; Guo, Z.J.; Wang, X.L.; Du, B.W.; Zhu, Z.F. *The Potential of the Oil and Gas Resources in Major Sedimentary Basins on the Qinghai-Xizang Plateau*; China Geological Publishing House: Beijing, China, 2004; pp. 167–168. (In Chinese with English Abstract)
12. Wang, J.; Fu, X.G.; Wei, H.Y.; Shen, L.J.; Wang, Z.; Li, K.Z. Late Triassic basin inversion of the Qiangtang Basin in northern Tibet: Implications for the closure of the Paleo-Tethys and expansion of the Neo-Tethys. *J. Asian Earth Sci.* **2022**, *227*, 105119. [[CrossRef](#)]
13. Wang, J.; Ding, J.; Wang, C.S.; Tan, F.W.; Chen, M.; Hu, P.; Li, Y.L.; Gao, R.; Fang, H.; Zhu, L.D.; et al. *Survey and Evaluation on Tibet Oil and Gas Resources*; Geological Publishing House: Beijing, China, 2009; pp. 11–223. (In Chinese with English Abstract)
14. Wang, J.; Fu, X.G.; Shen, L.J.; Tan, F.W.; Song, C.Y.; Chen, W.B. Prospect of the potential of oil and gas resources in Qiangtang Basin, Xizang (Tibet). *Geol. Rev.* **2020**, *66*, 1091–1113. (In Chinese with English Abstract)
15. Röhl, H.; Schmid-Röhl, A.; Oschmann, W.; Frimmel, A.; Schwark, L. The Posidonia Shale (Lower Toarcian) of SW-Germany: An oxygen-depleted ecosystem controlled by sea level and palaeoclimate. *Palaeogeogr. Palaeoclimatol. Palaeoecol.* **2001**, *165*, 27–52. [[CrossRef](#)]
16. Yi, H.S.; Chen, L.; Jenkyns, H.; Da, X.J.; Xia, M.Q.; Xu, G.W.; Ji, C.J. The Early Jurassic oil shales in the Qiangtang Basin, northern Tibet: Biomarkers and Toarcian oceanic anoxic events. *Oil Shale* **2013**, *30*, 441–455. [[CrossRef](#)]
17. Yi, H.S.; Lin, J.H.; Zhao, B.; Li, Y.; Shi, H. New Biostratigraphic Data of the Qiangtang Area in the Northern Tibetan Plateau. *Geol. Rev.* **2003**, *49*, 59–65. (In Chinese with English Abstract)
18. Chen, L.; Yi, H.S.; Hu, R.Z.; Zhong, H.; Zou, Y.R. Organic geochemistry of the Early Jurassic oil shale from the Shuanghu area in northern Tibet and the Early Toarcian oceanic anoxic event. *Acta Geol. Sin-Engl.* **2005**, *79*, 392–397.
19. Jenkyns, H.C. The early Toarcian (Jurassic) anoxic event: Stratigraphic, sedimentary, and geochemical evidence. *Am. J. Sci.* **1998**, *288*, 101–151. [[CrossRef](#)]
20. Jenkyns, H.C. Geochemistry of oceanic anoxic events. *Geochem. Geophys. Geosy.* **2010**, *11*, Q03004. [[CrossRef](#)]
21. Simms, M.J.; Ruffell, A.H. Synchronicity of climatic change and extinctions in the Late Triassic. *Geology* **1989**, *17*, 265–268. [[CrossRef](#)]
22. Jenkyns, H.C.; Jones, C.E.; Gröcke, D.R.; Hesselbo, S.P.; Parkinson, D.N. Chemostratigraphy of the Jurassic System: Applications, limitations and implications for palaeoceanography. *J. Geol. Soc.* **2002**, *159*, 351–378. [[CrossRef](#)]
23. Hornung, T.; Brandner, R. Biostratigraphy of the Reingraben Turnover (Hallstatt Facies Belt): Local black shale events controlled by the regional tectonics, climatic change and plate tectonics. *Facies* **2005**, *51*, 460–479. [[CrossRef](#)]
24. Dal Corso, J.; Gianolla, P.; Newton, R.J.; Franceschi, M.; Roghi, G.; Caggiati, M.; Raucsik, B.; Budai, T.; Haas, J.; Preto, N. Carbon isotope records reveal synchronicity between carbon cycle perturbation and the “Carnian Pluvial Event” in the Tethys realm (Late Triassic). *Global Planet. Chang.* **2015**, *127*, 79–90. [[CrossRef](#)]
25. Chen, L.; Mattioli, E.; Da, X.J.; Jenkyns, H.C.; Zhu, Z.X.; Xu, G.W.; Yi, H.S. Calcareous nannofossils from the Jurassic black shales in the Qiangtang Basin, Northern Tibet (China): New records of stratigraphic ages and palaeoceanography. *Newsl. Stratigr.* **2019**, *52*, 55–72. [[CrossRef](#)]
26. Yin, J.R. A revision and new data on the Jurassic ammonites from the Biluoco area, southern Qiangtang block (North Tibet). *Newsl. Stratigr.* **2022**, *55*, 1–19. [[CrossRef](#)]
27. Ma, A.L.; Hu, X.M.; Garzanti, E.; Marcelle, B.F.; Xue, W.W.; Han, Z.; Wang, P. Paleogeographic and tectonic evolution of Mesozoic Qiangtang basins (Tibet). *Tectonophysics* **2023**, *862*, 229957. [[CrossRef](#)]
28. Schootbrugge, B.; McArthur, J.M.; Bailey, T.R.; Rosenthal, Y.; Wright, J.D.; Miller, K.G. Toarcian oceanic anoxic event: An assessment of global causes using belemnite C isotope records. *Paleoceanography* **2005**, *20*, PA3008. [[CrossRef](#)]
29. Page, K.N. The Lower Jurassic of Europe: Its subdivision and correlation. In *The Jurassic of Denmark and Greenland*; Ineson, J.R., Surlyk, F., Eds.; Geological Survey of Denmark and Greenland: København, Denmark, 2003; pp. 23–59.
30. Suan, G.; Nikitenko, B.L.; Rogov, M.A.; Baudin, F.; Spangenberg, J.E.; Knyazev, V.G.; Glinskikh, L.A.; Goryacheva, A.A.; Adatte, T.; Riding, J.B.; et al. Polar record of Early Jurassic massive carbon injection. *Earth Planet. Sci. Lett.* **2011**, *312*, 102–113. [[CrossRef](#)]

31. da Rocha, R.B.; Mattioli, E.; Duarte, L.; Pittet, B.; Elmi, S.; Mouterde, R.; Cabral, M.C.; Comas-Rengifo, M.J.; Gómez, J.J.; Goy, A.; et al. Base of the Toarcian Stage of the Lower Jurassic defined by the Global Boundary Stratotype Section and Point (GSSP) at the Peniche section (Portugal). *Episodes* **2016**, *39*, 460–481. [[CrossRef](#)]
32. Subarkah, D.; Blades, M.L.; Collins, A.S.; Farkaš, J.; Gilbert, S.; Löhr, S.C.; Redaa, A.; Cassidy, E.; Zack, T. Unraveling the histories of Proterozoic shales through in situ Rb–Sr dating and trace element laser ablation analysis. *Geology* **2021**, *50*, 66–70. [[CrossRef](#)]
33. Nelson, D.R. An assessment of the determination of depositional ages for Precambrian elastic sedimentary rocks by U–Pb dating of detrital zircons. *Sediment. Geol.* **2001**, *141*, 37–60. [[CrossRef](#)]
34. Dickinson, W.R.; Gehrels, C.E. Use of U–Pb ages of detrital zircons to infer maximum depositional ages of strata: A test against a Colorado Plateau Mesozoic database. *Earth Planet. Sci. Lett.* **2009**, *288*, 115–125. [[CrossRef](#)]
35. Tera, F.; Wasserburg, G.J. U–Th–Pb systematics in lunar highland samples from the Luna 20 and Apollo 16 missions. *Earth Planet. Sci. Lett.* **1972**, *17*, 36–51. [[CrossRef](#)]
36. Rasbury, E.T.; Cole, J.M. Directly dating geologic events: U–Pb dating of carbonates. *Rev. Geophys.* **2009**, *47*. [[CrossRef](#)]
37. Roberts, N.M.; Drost, K.; Horstwood, M.S.; Condon, D.J.; Chew, D.; Drake, H.; Milodowski, A.E.; McLean, N.M.; Smye, A.J.; Walker, R.J.; et al. Laser ablation inductively coupled plasma mass spectrometry (LA-ICP-MS) U–Pb carbonate geochronology: Strategies, progress, and limitations. *Geochronology* **2020**, *2*, 33–61. [[CrossRef](#)]
38. Lan, Z.W.; Wu, S.T.; Wang, F.Y.; Liu, B.; Shi, K.B.; Sun, J.; Cao, R.; Li, X.H. A ca. 290 Ma hydrothermal calcite in Cambrian dolostone. *Mar. Pet. Geol.* **2023**, *147*, 106011. [[CrossRef](#)]
39. Cao, R.; Zhao, H.Q.; Lan, Z.W. Calcite U–Pb Geochronology Revealing Late Ediacaran–Early Paleozoic Hydrothermal Alteration in the Stenian–Tonian Carbonate of Northeastern North China Craton. *J. Earth Sci.* **2023**, *34*, 1724–1731. [[CrossRef](#)]
40. Lan, Z.W.; Wu, S.T.; Roberts, N.M.W.; Zhang, S.J.; Cao, R.; Wang, H.; Yang, Y.H. Geochronological and geochemical constraints on the origin of highly <sup>13</sup>Ccarb-depleted calcite in basal Ediacaran cap carbonate. *Geol. Mag.* **2022**, *159*, 1323–1334. [[CrossRef](#)]
41. Israelson, C.; Halliday, A.N.; Buchardt, B. U–Pb dating of calcite concretions from Cambrian black shales and the Phanerozoic time scale. *Earth Planet. Sci. Lett.* **1996**, *141*, 153–159. [[CrossRef](#)]
42. Coogan, L.A.; Parrish, R.R.; Roberts, N.M.W. Early hydrothermal carbon uptake by the upper oceanic crust: Insight from in situ U–Pb dating. *Geology* **2016**, *44*, 147–150. [[CrossRef](#)]
43. Lan, Z.W.; Roberts, N.M.W.; Zhou, Y.; Zhang, S.J.; Li, Z.S.; Zhao, T.P. Application of in situ U–Pb carbonate geochronology to Stenian–Tonian successions of North China. *Precambrian Res.* **2022**, *370*, 106551. [[CrossRef](#)]
44. Zhang, J.; Wang, J.; Zheng, B.; Sheng, Q.Y.; Wei, H.Y.; Shen, L.J.; Xiong, S.Y.; Mansour, A. Age assignment of dolomite in palaeo-reservoirs of the Qiangtang Basin: New evidence from palaeontology and carbonate in situ U–Pb dating. *Mar. Petrol. Geol.* **2023**, *158*, 106545. [[CrossRef](#)]
45. Horstwood, M.S.A.; Košler, J.; Gehrels, G.; Jackson, S.E.; McLean, N.M.; Paton, C.; Pearson, N.J.; Sircombe, K.; Sylvester, P.; Vermeesch, P.; et al. Community-Derived Standards for LA-ICP-MS U–(Th)–Pb Geochronology—Uncertainty Propagation, Age Interpretation and Data Reporting. *Geostand. Geoanal. Res.* **2016**, *40*, 311–332. [[CrossRef](#)]
46. Davis, D.W.; Rochín-Bañaga, H. A new Bayesian approach toward improved regression of low-count U Pb geochronology data generated by LA-ICPMS. *Chem. Geol.* **2021**, *582*, 120454. [[CrossRef](#)]
47. Rochín-Bañaga, H. U–Pb Dating of Fossils and Hydrogenic Minerals: Toward Practical Paleontological Chronometry. Ph.D. Thesis, University of Toronto, Toronto, ON, Canada, 2022.
48. Rochín-Bañaga, H.; Davis, D.W.; Moysiuk, J. U–Pb dating of belemnites and rugose corals: The potential for absolute dating of calcitic invertebrate fossils. *Chem. Geol.* **2023**, *644*, 121862. [[CrossRef](#)]
49. Li, Q.; Parrish, R.R.; Horstwood, M.S.A.; McArthur, J.M. U–Pb dating of cements in Mesozoic ammonites. *Chem. Geol.* **2014**, *376*, 76–83. [[CrossRef](#)]
50. Wang, J.; Fu, X.G. Sedimentary evolution of the Qiangtang Basin. *Geol. China* **2018**, *45*, 237–259. (In Chinese with English Abstract)
51. Kapp, P.; Yin, A.; Manning, C.E.; Murphy, M.; Harrison, T.M.; Spurlin, M.; Lin, D.; Xi-Guang, D.; Cun-Ming, W. Blueschist-bearing metamorphic core complexes in the Qiangtang block reveal deep crustal structure of northern Tibet. *Geology* **2000**, *28*, 19–22. [[CrossRef](#)]
52. Wang, J.; Fu, X.G.; Chen, W.X.; Tan, F.W.; Wang, Z.J.; Chen, M.; Zhuo, J.W. Chronology and geochemistry of the volcanic rocks in Woruo mountain region, northern Qiangtang Depression: Implications to the Late Triassic volcanic-sedimentary events. *Sci. China* **2008**, *51*, 194–205. [[CrossRef](#)]
53. Yi, F.; Yi, H.S.; Xia, G.Q.; Wu, C.H.; Li, G.J.; Cai, Z.H.; Li, N. Factors controlling the organic matter accumulation across the Pliensbachian–Toarcian transition in the Qiangtang Basin, Tibetan Plateau. *Mar. Petrol. Geol.* **2021**, *133*, 105304. [[CrossRef](#)]
54. Liu, M.; Ji, C.J.; Hu, H.W.; Xia, G.Q.; Yi, H.S.; Them, T.R., II; Sun, P.; Chen, D.Z. Variations in microbial ecology during the Toarcian Oceanic Anoxic Event (Early Jurassic) in the Qiangtang Basin, Tibet: Evidence from biomarker and carbon isotopes. *Palaeogeogr. Palaeoclimatol. Palaeoecol.* **2021**, *580*, 110626. [[CrossRef](#)]
55. Howarth, R.J. *The Ammonite Family Hildoceratidae in the Lower Jurassic of Britain*; The Palaeontographical Society: London, UK, 1992; pp. 69–70.
56. Nuriel, P.; Weinberger, R.; Kylander-Clark, A.R.C.; Hacker, B.R.; Craddock, J.P. The onset of the Dead Sea transform based on calcite age-strain analyses. *Geology* **2017**, *45*, 587–590. [[CrossRef](#)]
57. Shen, A.J.; Hu, A.P.; Cheng, T.; Liang, F.; Pan, W.Q.; Feng, Y.X.; Zhao, J.X. Laser ablation in situ U–Pb dating and its application to diagenesis-porosity evolution of carbonate reservoirs. *Petrol. Explor. Dev.* **2019**, *46*, 1127–1140. [[CrossRef](#)]

58. Roberts, N.M.W.; Rasbury, E.T.; Parrish, R.R.; Smith, C.J.; Horstwood, M.S.A.; Condon, D.J. A calcite reference material for LA-ICP-MS U–Pb geochronology. *Geochem. Geophys. Geosyst.* **2017**, *18*, 2807–2814. [[CrossRef](#)]
59. Cheng, T.; Zhao, J.X.; Feng, Y.X.; Pan, W.Q.; Liu, D.Y. In-situ LA-MC-ICPMS U–Pb dating method for low-uranium carbonate minerals. *Chin. Sci. Bull.* **2020**, *65*, 150–154. (In Chinese with English Abstract) [[CrossRef](#)]
60. Ludwig, K.R. *ISOPLLOT 3.0: A Geochronological Toolkit for Microsoft Excel*; Berkeley Geochronology Center: Berkeley, CA, USA, 2003.
61. Vermeesch, P. IsoplotR: A free and open toolbox for geochronology. *Geosci. Front.* **2018**, *9*, 1479–1493. [[CrossRef](#)]
62. Howarth, R.J.; McArthur, J.M. Statistics for Strontium Isotope Stratigraphy: A robust lowess fit to the marine Sr-isotope curve for 0 to 206 Ma, with look-up table for derivation of numeric age. *J. Geol.* **1997**, *105*, 441–456. [[CrossRef](#)]
63. Jakobs, G.K.; Smith, P.L.; Tipper, H.W. An ammonite zonation for the Toarcian (Lower Jurassic) of the North American Cordillera. *Can. J. Earth Sci.* **1994**, *31*, 919–942. [[CrossRef](#)]
64. Pálffy, J.; Smith, P.L. Synchrony between Early Jurassic extinction, oceanic anoxic event, and the Karoo-Ferrar flood basalt volcanism. *Geology* **2000**, *28*, 747–750. [[CrossRef](#)]
65. Kaufman, A.J.; Knoll, A.H. Neoproterozoic variations in the C-isotopic composition of seawater-stratigraphic and biogeochemical implications. *Precambrian Res.* **1995**, *73*, 27–49. [[CrossRef](#)]
66. Chen, L.; Mattioli, E.; Da, X.J.; Xu, G.W.; Zhu, Z.X.; Zhang, X.; Yi, H.S.; Jiang, S.J.; Wang, Y.S.; Jenkyns, H.C.; et al. Integrated carbon-isotope and calcareous nannofossil stratigraphy in the Middle Jurassic of Qinghai–Xizang (China). *Newsl. Stratigr.* **2023**, *56*, 405–421. [[CrossRef](#)]
67. Wang, Y.G.; Sun, D.L. The Triassic and Jurassic paleogeography and evolution of the Qinghai-Xizang (Tibet) Plateau. *Can. J. Earth Sci.* **1985**, *22*, 195–204. [[CrossRef](#)]
68. Wen, S.X. New stratigraphic materials in northern Tibet. *Acta Stratigr. Sin.* **1979**, *3*, 150–156. (In Chinese with English Abstract)
69. Yin, J.R.; Chandler, R.B. Aalenian to Lower Bajocian ammonites from the Qiangtang block (North Tibet). *Proc. Geol. Assoc.* **2015**, *464*, 17. [[CrossRef](#)]
70. Smith, P.L. Biostratigraphy and ammonoid fauna of the Lower Jurassic (Sinemurian, Pliensbachian and the Lowest Toarcian) of Eastern Oregon and Western Nevada. Ph.D. Thesis, McMaster University, Hamilton, ON, Canada, 1981; 435p.
71. Jakobs, G.K. Toarcian (Early Jurassic) ammonoids from western North America. *Geol. Surv. Can. Bull.* **1997**, *428*, 1–137.
72. Riding, J.B.; Walton, W.; Shaw, D. Toarcian to Bathonian (Jurassic) palynology of the Inner Hebrides, northwest Scotland. *Palynology* **1991**, *15*, 115–179. [[CrossRef](#)]
73. Correia, V.F.; Riding, J.B.; Duarte, L.V.; Fernandes, P.; Pereira, Z. The Early Jurassic palynostratigraphy of the Lusitanian Basin, western Portugal. *Geobios* **2018**, *51*, 537–557. [[CrossRef](#)]
74. Jin, X.; Shi, Z.Q.; Baranyi, V.; Kemp, D.B.; Han, Z.; Luo, G.M.; Hu, J.F.; He, F.; Chen, L.; Preto, N. The Jenkyns Event (early Toarcian OAE) in the Ordos Basin, North China. *Global Planet. Chang.* **2020**, *193*, 103273. [[CrossRef](#)]
75. Brooks, C.; Wendt, I.; Hart, S.R. Realistic use of 2-error regression treatments as applied to rubidium-strontium data. *Rev. Geophys.* **1972**, *10*, 551–577. [[CrossRef](#)]
76. Bartley, J.K.; Kah, L.C.; McWilliams, J.L.; Stagner, A.F. Carbon isotope chemostratigraphy of the Middle Riphean type section (Avzyan Formation, Southern Urals, Russia): Signal recovery in a fold-and-thrust belt. *Chem. Geol.* **2007**, *237*, 211–232. [[CrossRef](#)]
77. Kah, L.C.; Bartley, J.K.; Teal, D.A. Chemostratigraphy of the Late Mesoproterozoic Atar Group, Taoudeni Basin, Mauritania: Muted isotopic variability, facies correlation, and global isotopic trends. *Precambrian Res.* **2012**, *200*, 82–103. [[CrossRef](#)]
78. Derry, L.A.; Kaufman, A.J.; Jacobsen, S.B. Sedimentary cycling and environmental change in the Late Proterozoic: Evidence from stable and radiogenic isotopes. *Geochim. Cosmochim. Acta* **1992**, *56*, 1317–1329. [[CrossRef](#)]
79. McArthur, J.M.; Howarth, R.J.; Shields, G.A. Strontium isotope stratigraphy. In *The Geologic Time Scale*; Gradstein, F.M., Ogg, J.G., Schmitz, M., Ogg, G., Eds.; Elsevier: Amsterdam, NY, USA, 2020.
80. Caruthers, A.H.; Gröcke, D.R.; Smith, P.L. The significance of an Early Jurassic (Toarcian) carbon isotope excursion in Haida Gwaii (Queen Charlotte Islands), British Columbia, Canada. *Earth Planet. Sci. Lett.* **2011**, *307*, 19–26. [[CrossRef](#)]
81. Pálffy, J.; Parrish, R.R.; Smith, P.L. A U–Pb age from the Toarcian (Lower Jurassic) and its use for time scale calibration through error analysis of biochronologic dating. *Earth Planet. Sci. Lett.* **1997**, *146*, 659–675. [[CrossRef](#)]
82. Ma, A.L.; Hu, X.M.; Garzanti, E.; Han, Z.; Lai, W. Sedimentary and tectonic evolution of the southern Qiangtang basin: Implications for the Lhasa-Qiangtang collision timing. *J. Geophys. Res. Solid Earth* **2017**, *122*, 4790–4813. [[CrossRef](#)]
83. Merino-Tomé, O.; Della Porta, G.; Kenter, J.A.M.; Verwer, K.; Harris, P.; Adams, E.W.; Playton, T.; Corrochano, D. Sequence development in an isolated carbonate platform (Lower Jurassic, Djebel Bou Dahar, High Atlas, Morocco): Influence of tectonics, eustasy and carbonate production. *Sedimentology* **2012**, *59*, 118–155. [[CrossRef](#)]
84. Trecalli, A.; Spangenberg, J.; Adatte, T.; Follmi, K.B.; Parente, M. Carbonate platform evidence of ocean acidification at the onset of the early Toarcian oceanic anoxic event. *Earth Planet. Sci. Lett.* **2012**, *357*, 214–225. [[CrossRef](#)]
85. Sabatino, N.; Vlahovic, I.; Jenkyns, H.C.; Scopelliti, G.; Neri, R.; Prtoljan, B.; Velic, I. Carbon-isotope record and palaeoenvironmental changes during the early Toarcian oceanic anoxic event in shallow-marine carbonates of the Adriatic Carbonate Platform in Croatia. *Geol. Mag.* **2013**, *150*, 1085–1102. [[CrossRef](#)]
86. Han, Z.; Hu, X.M.; Kemp, D.B.; Li, J. Carbonate-platform response to the Toarcian Oceanic Anoxic Event in the southern hemisphere: Implications for climatic change and biotic platform demise. *Earth Planet. Sci. Lett.* **2018**, *489*, 59–71. [[CrossRef](#)]
87. Yin, J.R.; Gao, J.H.; Wang, Y.S.; Zhang, S.Q.; Zheng, C.Z.; Xu, D.B.; Bai, Z.D.; Sun, L.X.; Su, X. Jurassic ammonites in anoxic black shales from Sewa and Amdo, northern Tibet. *Acta Palaeontol. Sin.* **2006**, *45*, 311–331. (In Chinese with English Abstract)

- 
88. Kemp, D.B.; Coe, A.L.; Cohen, A.S.; Schwark, L. Astronomical pacing of methane release in the Early Jurassic period. *Nature* **2005**, *437*, 396–399. [[CrossRef](#)]
  89. Kemp, D.B.; Baranyi, V.; Izumi, K.; Burgess, R.D. Organic matter variations and links to climate across the early Toarcian oceanic anoxic event (T-OAE) in Toyora area, southwest Japan. *Palaeogeogr. Palaeocl.* **2019**, *530*, 90–102. [[CrossRef](#)]

**Disclaimer/Publisher’s Note:** The statements, opinions and data contained in all publications are solely those of the individual author(s) and contributor(s) and not of MDPI and/or the editor(s). MDPI and/or the editor(s) disclaim responsibility for any injury to people or property resulting from any ideas, methods, instructions or products referred to in the content.